Pure Appl. Geophys. 174 (2017), 4329–4342

DOI 10.1007/s00024-017-1671-2

Pure and Applied Geophysics

The Effect of Ignoring Earth Curvature on Near-Regional Traveltime Tomography and Earthquake Hypocentral Determination

Chao-ying Bai,[1,2] Xing-wang Li,[1] Di Wang,[1] and Stewart Greenhalgh[3]

Abstract—Earthquake hypocenter determination and traveltime tomography with local earthquake data are normally conducted using a Cartesian coordinate system and assuming a flat Earth model, but for regional and teleseismic data Earth curvature is incorporated and a spherical coordinate system employed. However, when the study region is from the local to near-regional scale (1°–4°), it is unclear what coordinate system to use and what kind of incorrect anomalies or location errors might arise when using the Cartesian coordinate frame. In this paper we investigate in a quantitative sense through two near-regional crustal models and five different inversion methods, the hypocenter errors, reflector perturbation and incorrect velocity anomalies that can arise due to the selection of the wrong coordinate system and inversion method. The simulated inversion results show that the computed traveltime errors are larger than 0.1 s when the epicentral distance exceeds 150 km, and increases linearly with increasing epicentral distance. Such predicted traveltime errors will result in different patterns of incorrect velocity anomalous structures, a perturbed Moho interface for traveltime tomography and source position which deviate for earthquake locations. The maximum magnitude of a velocity image artifact is larger than 1.0% for an epicentral distance of less than 500 km and is up to 0.9% for epicentral distances of less than 300 km. The earthquake source location error is more than 2.0 km for epicentral distances less than 500 km and is up to 1.5 km for epicentral distances less than 300 km. The Moho depth can be in error by up 1.0 km for epicentral distances of less than 500 km but is less than 0.5 km at distances below 300 km. We suggest that spherical coordinate geometry (or time correction) be used whenever there are ray paths at epicentral distances in excess of 150 km.

Key words: Cartesian coordinate system, spherical coordinate system, multiple ray tracing, traveltime error, simultaneous inversion, earthquake location.

1. Introduction

It is common practice to assume a flat Earth model and use a Cartesian coordinate system when determining hypocentral coordinates of local earthquakes and conducting local earthquake traveltime tomography. When dealing with regional (or global) traveltime tomography (or determination of earthquake hypocenters), Earth curvature is taken into account and a spherical coordinate system is employed. For example, Müller (1971) conducted transformation from spherically symmetrical Earth into a vertically inhomogeneous half-space to obtain an Earth-flattening approximation for regional body waves, Chapman (1973) investigated a simple class of power law transformations between spherical and plane models for determining the effect of the Earth-flattening approximation in body wave studies. Gorman et al. (2002) used a modified ray-theoretical traveltime inversion routine that respects the spherical geometry of the Earth in their lithoprobe deep probe and southern Alberta refraction experiment data sets. Bozdağ and Trampert (2010) applied ray-theoretical and finite frequency approximations for crustal correction in surface wave tomography. Huang et al. (2013) developed a feasible global ray tracing algorithm for 3-D spherical Earth model based on multistage irregular shortest-path method (Multistage ISPM), in which the traveltimes and corresponding raypaths for 49 kinds of global phases can be computed, with 0.1 s absolute time error when compared with AK135 traveltime table (Kennett et al. 1995). Furthermore, the actual Earth is not a perfect sphere but rather an ellipsoid, it is constructive to conduct ray tracing directly in ellipsoidal coordinate system (Li et al. 2017), in which we extend the

[1] Department of Geophysics, School of Geology Engineering and Geomatics, Chang'an University, Xi'an 710054, China. E-mail: baicy@chd.edu.cn

[2] Institute of Computing Geophysics, Chang'an University, Xi'an 710054, China.

[3] Department of Geosciences, King Fahd University of Petroleum and Minerals, Dhahran 31261, Saudi Arabia.

functional of the multistage irregular shortest-path method, previously formulated for the Spherical Earth model (Huang et al. 2013), to the ellipsoidal Earth model to successfully trace multi-phase seismic arrivals. Furthermore, the comparison tests indicate that the traveltime differences between the ellipsoidal and the spherical coordinate ray tracing methods cannot be ignored for direct P and S arrivals, reflected PcP and ScS arrivals and reflected and converted PcS and ScP arrivals.

However, there is little literature concerning question of the cutoff range, from local to near-regional earthquakes of between 100 and 500 km, as to what is the effect of selecting the wrong coordinate system. Snoke and Lahr (2001) discussed the problem, for earthquake location of determining the epicentral at which the Earth can no longer be treated as flat. They suggested that one should use an appropriate model with flat Earth ray tracing for small epicentral distances and spherical Earth ray tracing (such as the IASPI91-package-generated spherical Earth traveltime tables, Kennett and Engdahl 1991) beyond a chosen threshold distance [such as the crossover distance, where the arrival times for refracted crustal (Pg) and upper mantle (Pn) rays are the same]. They proposed that this is a reasonable compromise that provides sufficient accuracy when locating earthquakes with arrivals ranging from local to regional distances. As far as we know, there has been little subsequent discussion and analysis of the issue. Previously, several authors examined the influence of predicted traveltime errors (or picking errors) on later arrival traveltime tomography. For example, Squires et al. (1992) investigated the effects of statics on velocity tomography and found that traveltime errors of 2% in forwarding modeling (or in picking) can cause later tomographic velocity error (or artifacts) of up to 7%. Gruber (1998) also analyzed the influence of data errors on the final imaging results and concluded that the velocity contrast could be masked by relatively moderate data errors. In this situation the inversion image (or located earthquake hypocenters or reflector geometry) could not give the true distribution in target areas having relatively small velocity contrasts. Gorman (2002) used a cylindrical coordinate system rather than a Cartesian coordinate system for ray tracing to remedy Earth's curvature in his lithospheric-scale controlled-source traveltime tomography and concluded that seismic refraction surveys greater than $\sim$350 km in length should take into consideration of effects of Earth's curvature.

There are two contributing factors to arrival time errors in traveltime tomography (or determination of earthquake locations): one is the theoretical (or predicting) traveltime error in forward modeling, and the other is the picking error for a specific arrival in the seismograms. Here, we will concentrate on the first type of time error on subsequent traveltime tomography and earthquake hypocenter determinations. In other words, we wish to study the timing errors introduced by the forward modeling (or ray tracing), due to selection of an unsuitable coordinate system. Furthermore, we will evaluate the subsequent magnitude of image artifacts (or deviations in the tomograms) which along with errors in hypocentral coordinates can be introduced when an unsuitable coordinate system is used.

2. *Methodology*

For forwarding modeling, two irregular shortest-path ray tracing methods are used to predict the direct P and reflected PP arrivals: one is used to predict multi-phase arrivals in the Cartesian coordinate frame (referred to as the Multistage ISPM_Car, Bai et al. 2010), and the other in spherical coordinates (referred to as the Multistage ISPM_Sph, Huang et al. 2013). The computational accuracy and efficiency for the Multistage ISPM_Car ray tracing method was compared with the multistage fast marching method (referred to as the multistage FMM of Rawlinson and Sambridge 2004) and found to be very similar, with no unfavorable results (Bai et al. 2010). The Multistage ISPM_Sph ray tracing method was tested against the AK135 (Kennett et al. 1995) global traveltime tables, and absolute traveltime errors of less than 0.1 s were observed for 49 kinds of global seismic phases (Huang et al. 2013).

For the tomographic inversion, we used our previously developed simultaneous inversion algorithm which recovers not only the velocity model but also the source hypocenter (see Huang et al. 2012) and

optionally also the interface geometry (triple model parameter inversion—see Bai et al. 2015). Both the subspace inversion solver (Kennett et al. 1988) and the damped minimum norm and constrained least squares solver (Zhou et al. 1992) can be used.

3. *Traveltime Errors Between Flat Earth and Spherical Earth Ray Tracing Methods*

To analyze the Earth curvature problem, we selected a near-regional model (see lower panel of Fig. 1). The model dimensions are 4° × 4° × 60 km, in which a horizontal Moho discontinuity is located at a depth of 45 km. The upper panel of Fig. 1 is 3-D Cartesian coordinate representation of the model, converted from the 3-D spherical model shown in the lower diagram. There are 30 randomly distributed sources located over the depth range of 10–30 km, and 81 receivers are uniformly arranged at the top surface of the model. In the model parameterization, cells of 0.2° × 0.2° × 10 km and 20 × 20 × 10 km were used to define the 3-D spherical and Cartesian coordinate models, respectively. The secondary node spacing (0.2 km) is the same for both models (computational accuracy consideration). The P-wave model here is the AK135 velocity model for the 3-D spherical coordinates and the flat AK135 velocity model for the 3-D Cartesian coordinates (here the flat AK135 velocity model is obtained by flatting the spherical AK135 velocity model into flat Earth model, for the spherical AK135 model the velocity is changed with radius, but for the flat AK135 model, the velocity is varied with depth).

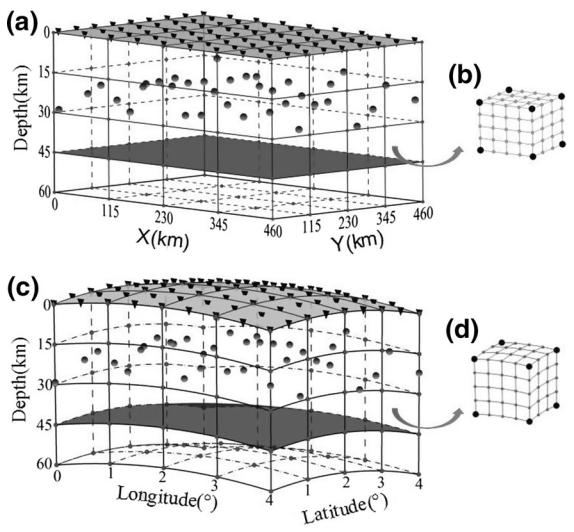

Figure 1
Model parameterization in two different models with located sources (large gray dots) and receivers (black triangles) (**a** 3-D Cartesian coordinate model diagram, **c** 3-D spherical coordinate model; **b** and **d** cells used to define Cartesian and spherical models). In **b** and **d**, the large black and small gray dots are referred to as primary and secondary nodes, respectively

Figure 2 shows the number of rays (direct P and Moho reflected PmP arrivals) vs. epicentral distance ranges for the source–receiver layouts of Fig. 1. For direct P arrivals, they include direct Pg for shorter epicentral distance and mantle refracted Pn for longer epicentral distance. The crossover distance for Pg and Pn can be seen in later discussion. To concise presentation, here we refer both Pg and Pn as to P. From Fig. 2 it is clear that most of the rays (75%) fall in the epicentral distance range of 100–400 km, and very few rays (less than 5%) come from epicentral distances greater than 500 km.

For later traveltime tomography and earthquake hypocenter determination, here we only consider P and PmP arrivals. Figure 3 displays the traveltime differences ($T_{Car} - T_{Sph}$) calculated by the multistage ISPM_Car and the ISPM_Sph ray tracing methods for the source–receiver layouts indicated in Fig. 1. In general, the traveltimes predicted by the multistage

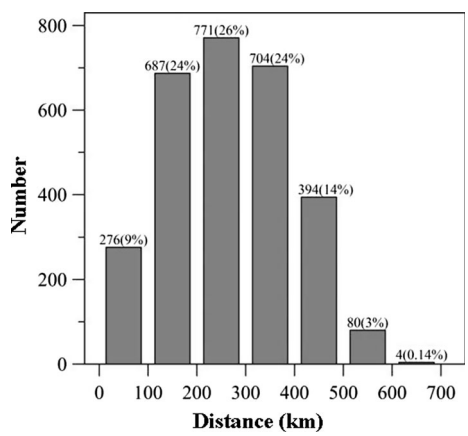

Figure 2
Ray numbers vs. epicentral distance for source–receiver layouts shown in large-scale model case (Fig. 1). The numbers at the top of the histogram are the numbers of rays for this distance range, the percentages in brackets are the percentages of rays occurring in this range

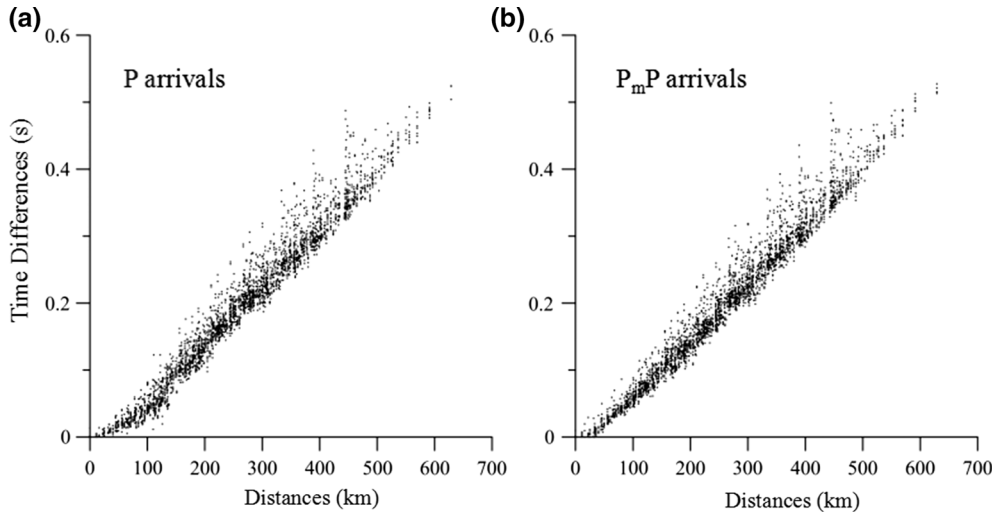

Figure 3
Traveltime differences calculated by the Multistage ISPM_Car and the Multistage ISPM_Sph ray tracing methods for the source–receiver layout in large-scale model case (Fig. 1) (**a** refracted P arrivals and **b** reflected PmP arrivals)

ISPM_Car ray tracing method are greater than those of the multistage ISPM_Sph ray tracing method, for both P and PmP phases. From Fig. 3, the traveltime differences between the two different coordinate ray tracing methods are observed to increase roughly linearly with increasing epicentral distances and are greater than 0.1 s when the epicentral distance exceeds 150 km for both the P and PmP arrivals.

4. *Simulation Tests for Traveltime Tomography and Hypocenter Positioning*

In these simulations, we present five tests that assess the incorrect images and location errors that can be introduced by using a flat Earth geometry (Cartesian coordinates) to represent data acquired on a spherical Earth model. The "observed" times here are those that have been simulated using spherical Earth ray tracing in spherical coordinates (Multistage ISPM-Sph), but we use the incorrect flat Earth ray tracing and inversion in Cartesian coordinates to recover the velocity model, reflector geometry and determine earthquake hypocenters. We expect to obtain inaccurate images (artifacts) and source mislocations using the inappropriate frame, assuming that the initial (input) model parameters are for a more accurate spherical model of the Earth.

From this point of view, the following simulations assume that the P and PmP traveltimes predicted by the multistage ISPM_Sph ray tracing method are the simulated real data (no random noise added). The five inversions conducted under the Cartesian coordinate flat Earth geometry assess the percentage of each image and/or source deviation that can be attributed to traveltime errors in the forward modeling.

4.1. *Large-Scale Model*

The large-scale model and source–receiver layout are shown as in Fig. 1. The input velocity model is the flat AK135 P-wave model, and the source locations and the Moho reflecting interface are fixed in their correct positions. Therefore, the incorrect velocity anomalies, source location errors and reflector perturbation can all be attributed to the traveltime errors introduced from the forwarding modeling (or ray tracing). The five inversion methods applied (Bai et al. 2015) are: (1) traveltime tomography used only to update the velocity model (referred to as V_{Invert}); (2) earthquake locations where the velocity model is known (referred to as S_{Invert}); (3) traveltime tomography used only to update the reflector geometry

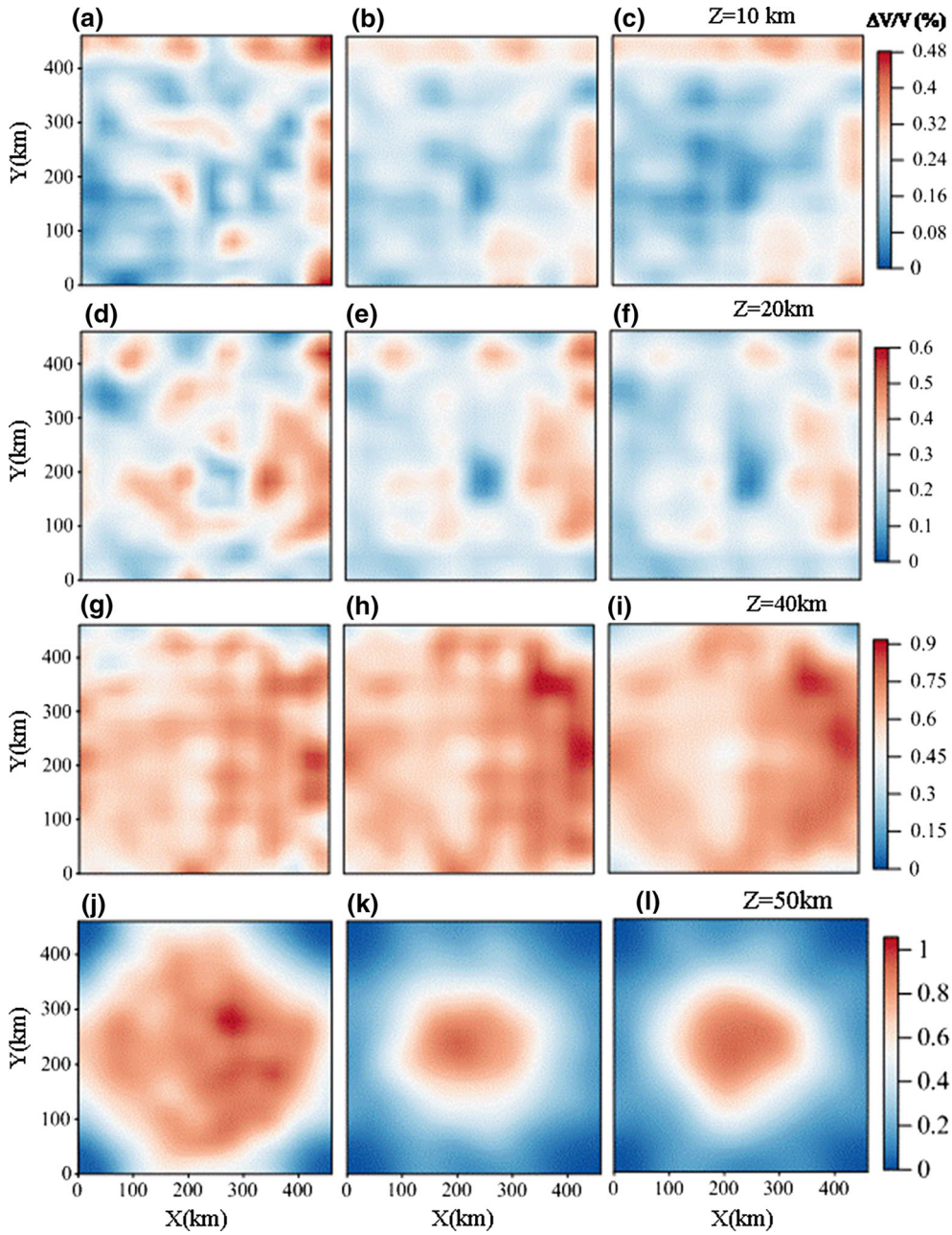

Figure 4
Velocity reconstruction for three different inversion methods on several horizontal planes at the depth levels in large-scale model case (left panels results for V_{Invert} method; middle panels results for $V + R$ method and right panels results for $V + S$ method)

(referred to as R_{Invert}); (4) simultaneous traveltime tomography used to update both the velocity field and the reflector geometry (referred to as V + R) and (5) traveltime tomography used to simultaneously update both the velocity field and the source positions (referred to as V + S). To concentrate just on the local to near-regional scale in these five inversion tests, we disregard the records from epicentral distances greater than 500 km for both P and PmP arrivals. The traveltime RMS residuals for five

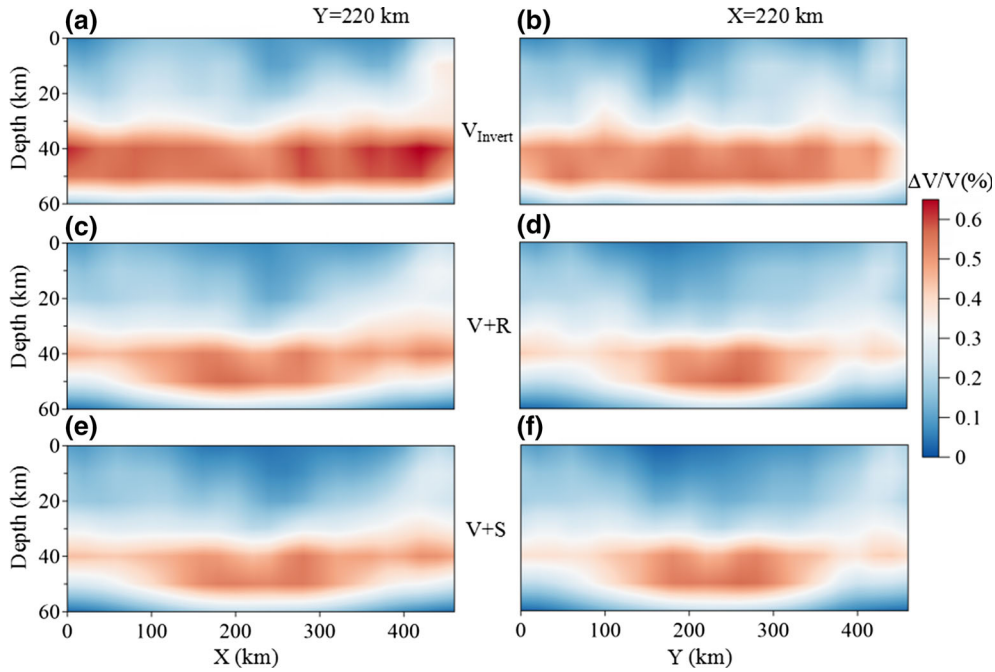

Figure 5
Velocity reconstruction for three different inversion methods on two cross sections in large-scale model case (left panels $Y = 220$ km; right panels $X = 220$ km; upper panels results for V_{Invert} method; middle panels results for $V + R$ method and lower panels results for $V + S$ method)

inversion approaches start at 0.24 s and converge nearly at 0.03 s after 15 iteration times.

Figure 4 shows the incorrect velocity anomalies $(V_{\text{Invert}} - V_{\text{Real}})/V_{\text{Real}} \times 100\%$ introduced by the traveltime errors in the forward modeling for the three velocity reconstruction methods at four horizontal depth levels. If there were no traveltime errors in the ray tracing process, then there would not be any incorrect anomalies in the reconstructed velocity fields. However, several patterns of incorrect anomalous velocity structures are observed at the different depth levels in the tomograms, regardless of which inversion approach was used. The image artifacts observed for the three different methods (V_{Invert}, $V + R$ and $V + S$) have similar patterns, especially the $V + R$ and $V + S$ simultaneous inversion methods. This is due to the same source–receiver layouts, regardless of single parameter or double parameters updated. The velocity errors are seen to increase with depth, with the maximum at about 1.0% (see the lower panels of Fig. 4). Such errors cannot be ignored in real applications.

Figure 5 displays incorrect anomalous patterns for two orthogonal cross sections. The patterns are similar for each of the three inversion approaches, with the most significant incorrect anomalous structure appearing around the Moho reflection interface. The maximum magnitude of the incorrect anomaly is about 0.6%. As seen from Fig. 5, for single parameter inversion (V_{Invert}) the inaccurate traveltime errors were totally mapped into incorrect velocity anomalies around the Moho reflection interface, with a large-scaled anomaly and a high magnitude of anomaly, and for double parameter inversion ($V + S$, or $V + R$) the partial inaccurate traveltime errors were mapped into relatively small-scaled incorrect velocity anomalies around the Moho reflection interface, and the rests go to adjust the source hypocenters or perturb the reflector geometry (see later Sect. 5).

Two methods were applied for earthquake hypocenter determination in a Cartesian coordinate frame. One positions earthquake hypocenters with a true velocity model and the other uses simultaneous inversion for updating both the velocity model and

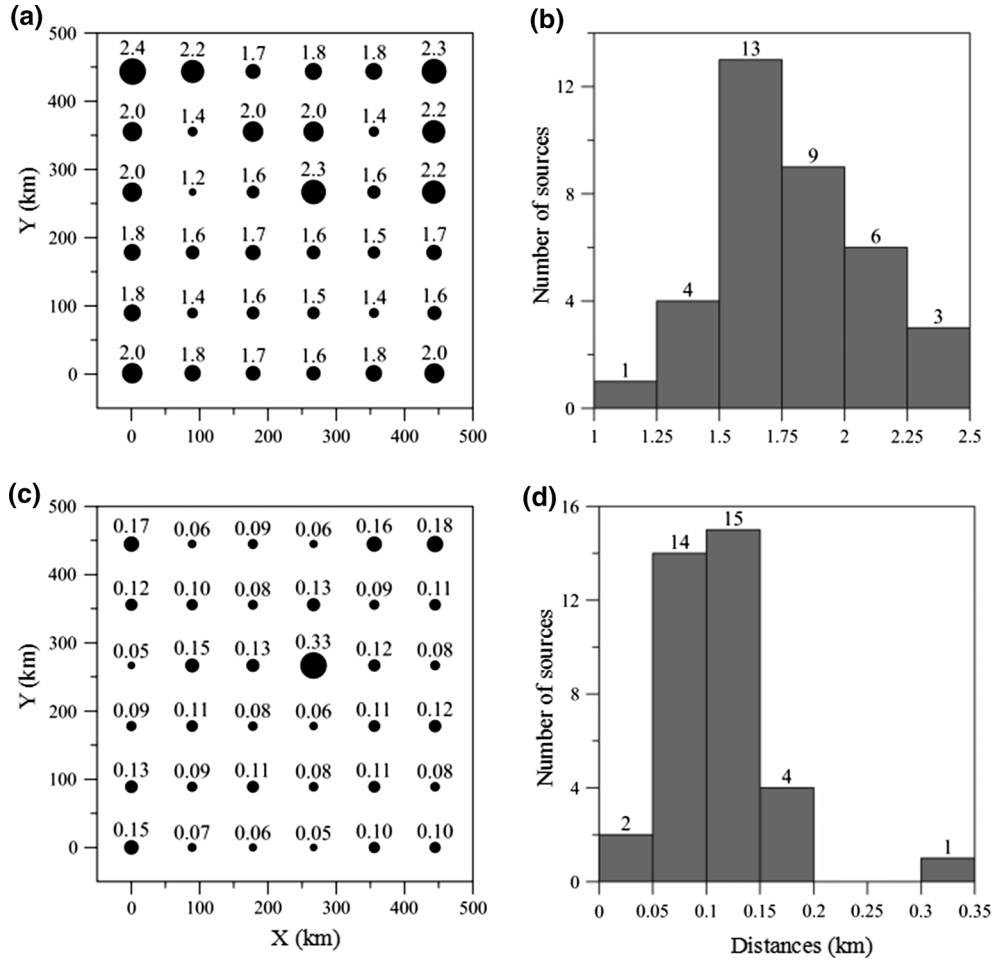

Figure 6
Perturbed distances from the true source positions for the S_{Invert} method in large-scale model case (upper panels) and $V + S$ method (lower panels). The location errors were projected onto the horizontal plane (left panels) and corresponding source numbers vs. location error (right panels)

the source positions (Bai et al. 2015). The initial velocity model and the initial source positions are considered to be the actual ones. Similar to the discussion above, if there are no traveltime errors in the ray tracing process, and then there would not be any perturbations from the deduced source locations from the true positions. However, Fig. 6 shows the updated hypocenters diverge from the true positions by 1.0–2.5 km with the S_{Invert} method (see upper panels in Fig. 6), but only from 0.0 to 0.35 km (most within 0.2 km, see lower panels in Fig. 6) with the $V + S$ simultaneous inversion method. For the latter case, more effort is expended in updating the velocity field (see Figs. 4, 5).

The two method results in a distortion in the Moho interface depth recovery. Rather than being flat, the Moho is domed (Fig. 7a, b), regardless of whether the R_{Invert} or $V + R$ method was employed. The maximum reflector perturbation from the true depth is 1.2 km for the R_{Invert} method, but only 0.5 km for the $V + S$ method (see Fig. 7c, d).

4.2. Small-Scale Model

In the previous section we discussed the inaccurate images and hypocenter location errors introduced by errors in the modeled traveltimes due to an unsuitable Cartesian coordinate ray tracing method,

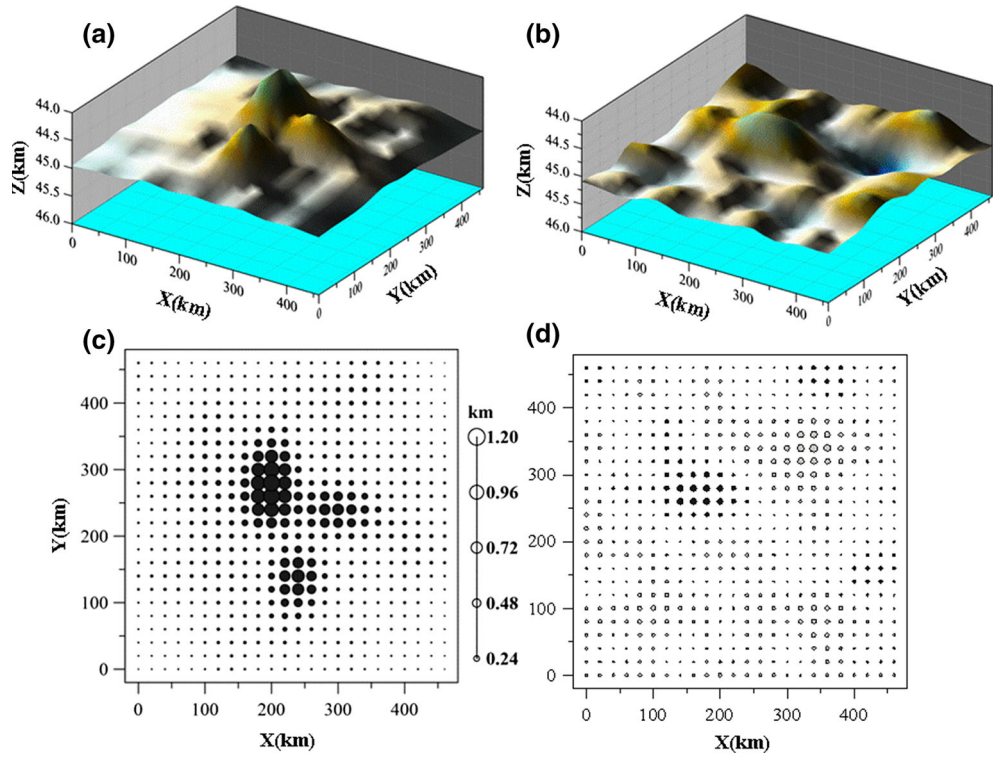

Figure 7
Updated Moho interface depth for the R_{Invert} (**a**) and $V + R$ (**b**) methods and the differences between updated and true depths (**c**, **d**) in large-scale model case. In **c** and **d**, the gray or black circles indicate positive and negative vertical distances between the updated and true reflector and the radius of the circle denotes corresponding magnitude

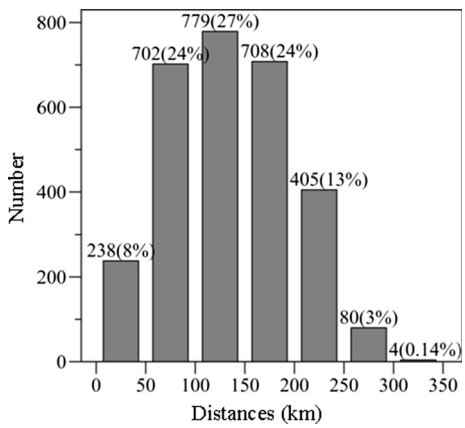

Figure 8
Ray numbers vs. epicentral distance for source–receiver layouts shown in small-scale model case. The numbers at the top of the histogram are the numbers of rays for this distance range, the percentages in brackets are the percentages of rays occurring in this range

for a near-regional 3-D velocity model (Fig. 1) and concluded that such discrepancies cannot be ignored in real applications. The question remains as to the earthquake distance range at which such incorrect images and mislocations can be ignored. To this end, we reduced dimensions of the 3-D model (Fig. 1) to half size in the horizontal direction and kept the other parameters unchanged, thereby obtaining a relatively small 3-D model (model scale: $2° \times 2° \times 60$ km). The source–receiver layouts are also reduced to half size in the horizontal direction and kept the source focuses unchanged. In this reduced 3-D model, more than half (68.0%) of the rays exceed an epicentral distance of 100 km and 16% go beyond 200 km (Fig. 8). The traveltime RMS residuals for five inversion approaches start at 0.1 s and converge roughly at 0.025 s after 15 iteration times.

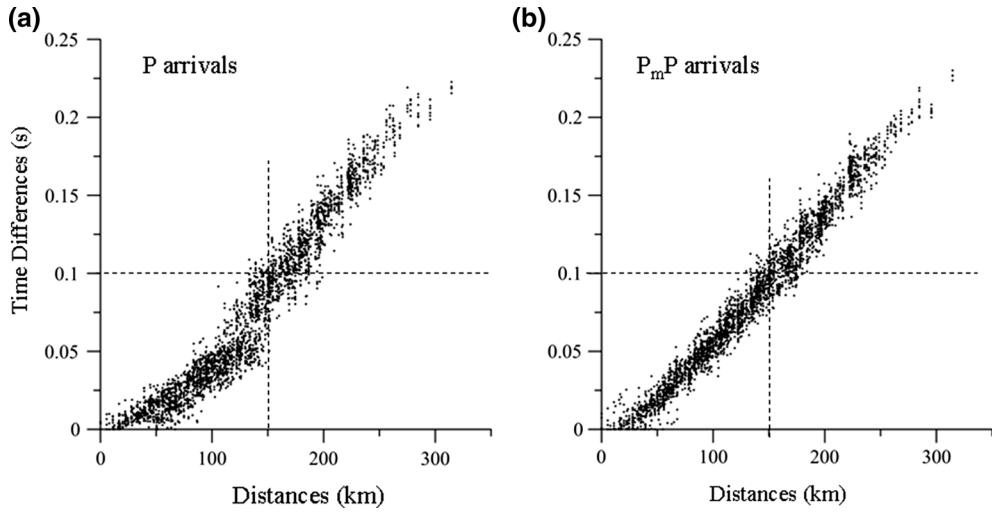

Figure 9
Traveltime differences calculated by the Multistage ISPM_Car and the Multistage ISPM_Sph ray tracing methods for the source–receiver layout in small-scale model case (**a** refracted P arrivals and **b** reflected PmP arrivals)

Figure 9 depicts the traveltime differences ($T_{\mathrm{Car}} - T_{\mathrm{Sph}}$) calculated by the multistage ISPM_Car and the ISPM_Sph ray tracing methods for the small-scale model. In general, the traveltimes predicted by the multistage ISPM_Car ray tracing method are greater than those of the multistage ISPM_Sph ray tracing method, for both P and PmP phases. From Fig. 9a, it is clearly shown that the crossover distance for direct P (Pg) and refracted P (Pn) is at about 125 km. The former one (Pg) has a relative small slope, but the latter one (Pn) has a relative large slope. Note that for surface focus in IASP91 velocity model, Moho at 35 km in depth, this crossover distance is 82 km, (Snoke and Lahr 2001). The crossover distance will increase with increasing focus depth. In our case, the source focuses range from 10 to 30 km in depth and Moho depth is 45 km in AK135 velocity model. So the crossover distance of 125 km in our case is reasonable. It can be also observed from Fig. 9, the traveltime differences are greater than 0.1 s when the epicentral distance exceeds 150 km for both P and PmP arrivals.

We repeated the five inversion method trials in parallel to those presented similar to the Sect. 4.1 (large-scale model case). Figure 10 shows the incorrect velocity anomalies introduced by the traveltime errors in the forward modeling for the three velocity reconstruction methods at four horizontal depth levels. Similar to the large-scale model case, several patterns of anomalous velocity structures are observed at the different depth levels in the tomograms, regardless of which inversion approach was used. The incorrect images observed for the three different methods (V_{Invert}, $V + R$ and $V + S$) have similar patterns, especially the $V + R$ and $V + S$ simultaneous inversion methods. Meanwhile, the updated velocity values are in positive direction (increasing velocity value at different depth level), due to positive traveltime errors ($T_{\mathrm{Car}} - T_{\mathrm{Sph}} > 0.0$). Comparing with the large-scale model case (Fig. 4), the incorrect anomalies have similar patterns, especially for depth of 40 and 50 km, but with reduced anomalous magnitude. Figure 11 displays incorrect anomalies for two orthogonal cross sections, which is very similar to the large-scale model case (Fig. 5), except for a basin-type high-velocity anomaly appears in central region near the top surface of the model. The patterns are similar for each of the three inversion approaches, with the most significant incorrect anomalous structure appearing around the Moho reflection interface.

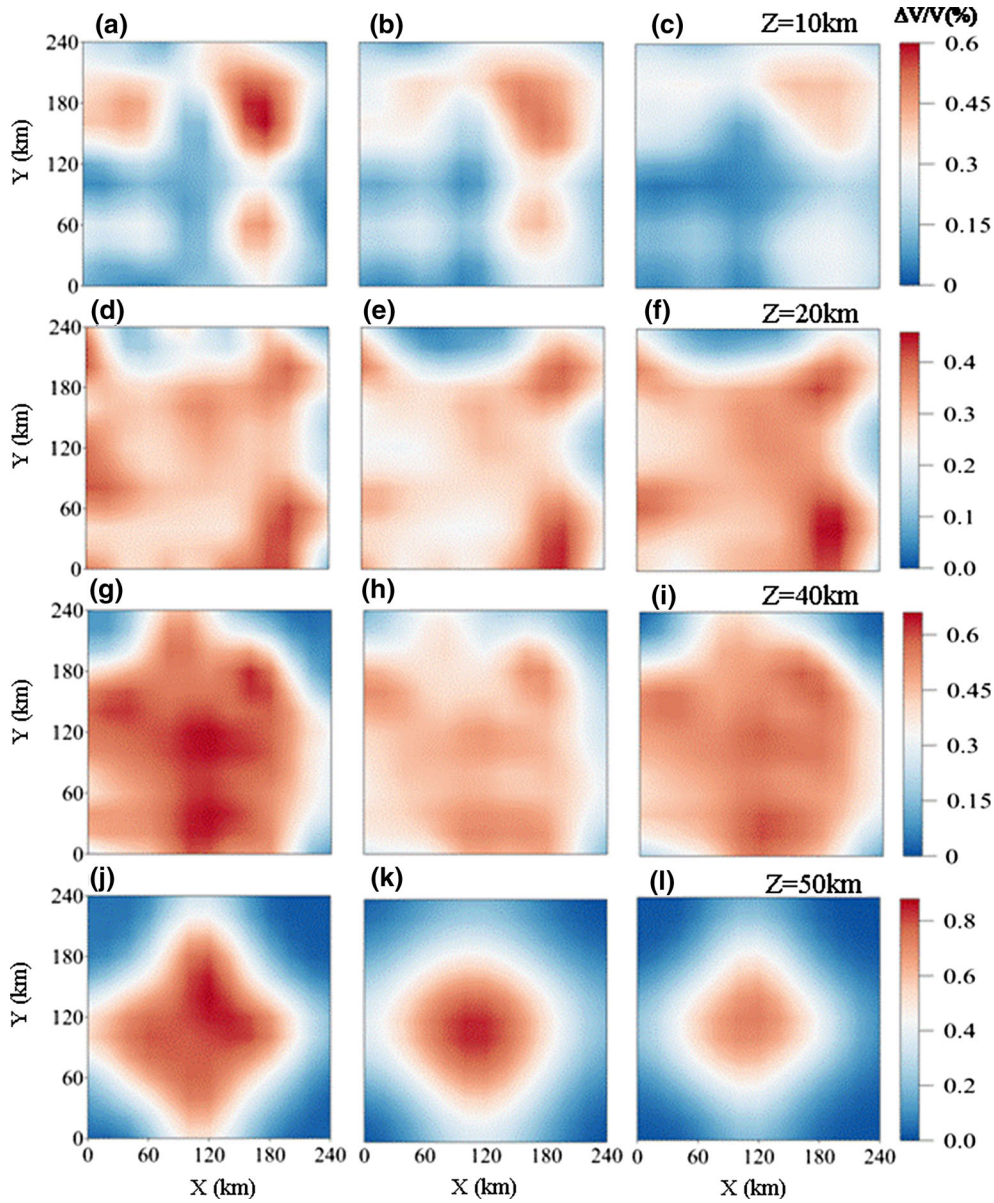

Figure 10
Velocity reconstruction for three different inversion methods on several horizontal planes at the depth levels for small-scale model case (left panels: results for V_{Invert} method; middle panels: results for $V + R$ method and right panels: results for $V + S$ method)

Similar to the large-scale model case, Fig. 12 shows the updated hypocenters diverge from the true positions by 0.4 –1.3 km with the S_{Invert} method (see upper panels in Fig. 12), but only from 0.0 to 0.25 km (most within 0.2 km, see lower panels in Fig. 12) with the $V + S$ simultaneous inversion method. Figure 13 shows a distortion in the Moho interface depth recovery for two (R_{Invert} and $V + R$) methods. Rather than being flat, the Moho is domed (Fig. 13a) or basined (Fig. 13b). The maximum reflector perturbation from the true depth is +0.45 km (upper perturbation) for the R_{Invert}

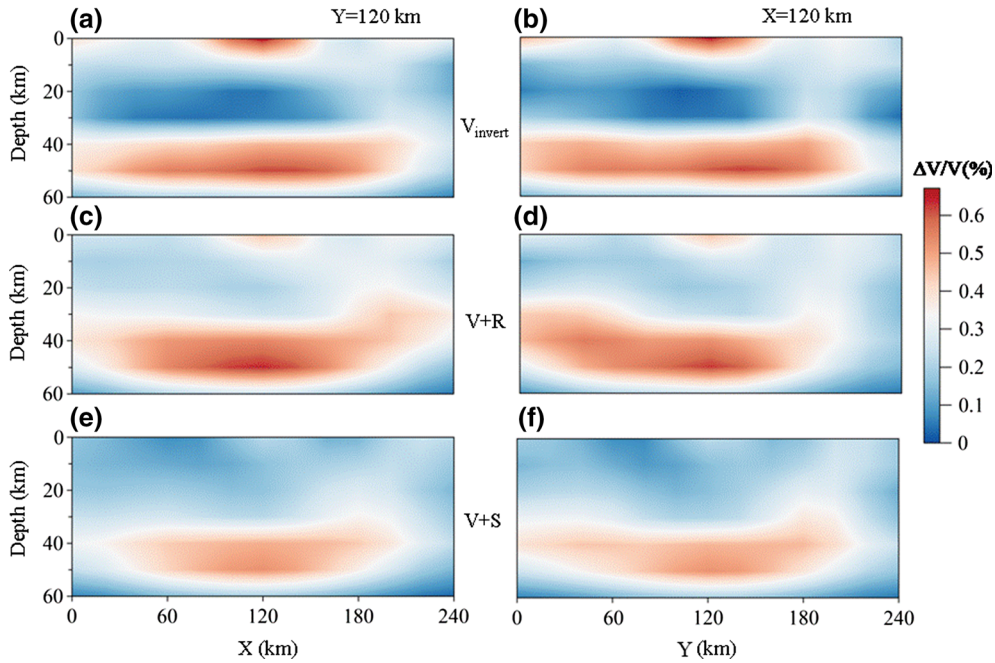

Figure 11
Velocity reconstruction for three different inversion methods on two cross sections in small-scale model case (left panels $Y = 220$ km; right panels $X = 220$ km; upper panels: results for V_{Invert} method; middle panels: results for $V + R$ method and lower panels: results for $V + S$ method)

method, but only −0.35 km (down perturbation) for the $V + S$ method (see Fig. 13c, d).

To quantitatively analyze the inverted results for the two models, Table 1 gives the combined results for the two model cases. Even for this relatively small model, the incorrect velocity anomalies, Moho depth perturbations and inaccurate source locations introduced by the errors in the modeled traveltimes from flat Earth ray tracing cannot be neglected. We conclude that if there is a certain fraction (e.g., 20%) of the rays with an epicentral distance greater than 150 km, then either spherical coordinates and an appropriate ray tracing scheme should be employed, or the traveltimes should be corrected to reduce the errors if one still wishes to conduct traveltime tomography or earthquake hypocenter determination within the Cartesian coordinate system frame. Otherwise, inversion artifacts and location inaccuracies will be introduced, regardless of the traveltime tomography algorithm or earthquake location method used. Such observations are similar to those of Snoke and Lahr (2001) but more strictly demonstrated here.

5. Discussion and Conclusions

There are sufficient differences in traveltime tomography and earthquake hypocenter determination in the near-regional distance range (150–500 km, or even 150–300 km), if we use different coordinate systems (i.e., Cartesian or spherical). The two near-regional crustal velocity models (including a Moho reflecting interface) constructed here have quantitatively examined the differences caused by their coordinate system through five different inversion approaches. For the specific source–receiver layout used, we analyzed the incorrect anomalous velocity patterns, Moho depth fluctuations and hypocentral location errors. In the larger model, which extends out to epicentral distances of 500 km, the

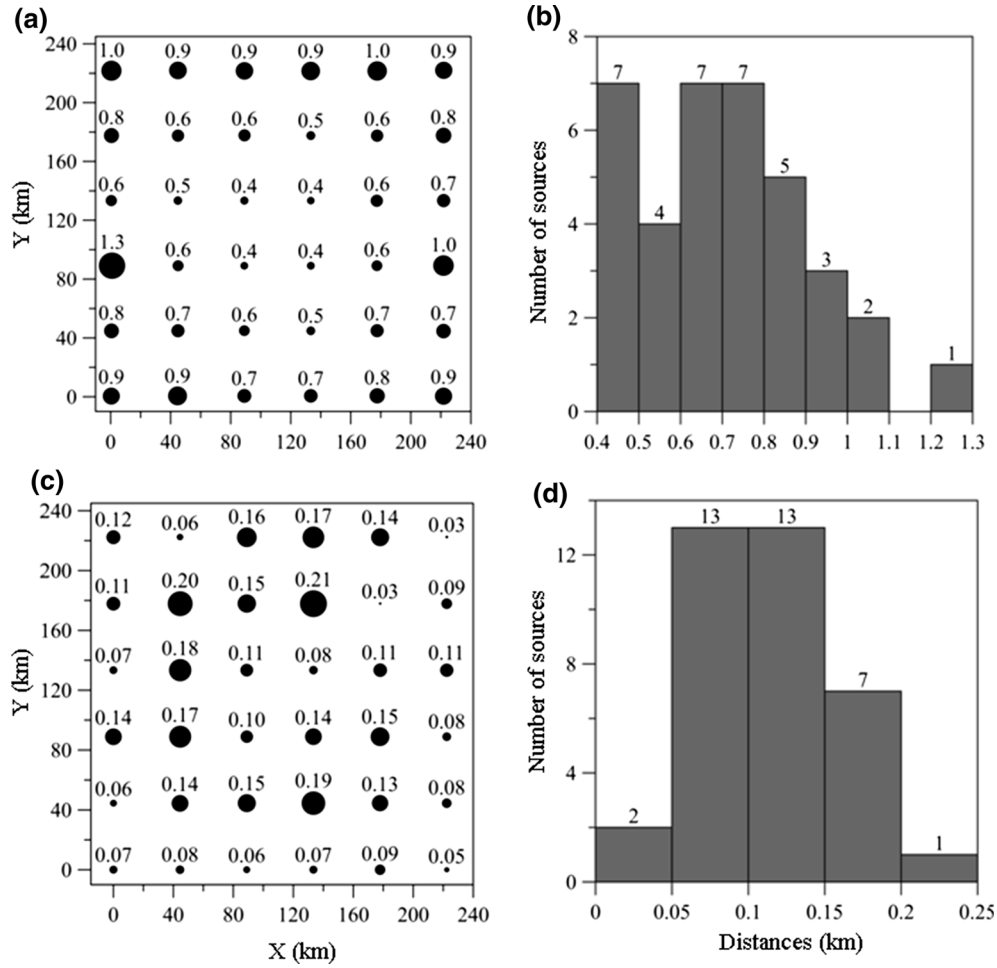

Figure 12
Perturbed distances from the true source positions for the S_{Invert} method (upper panels) and $V + S$ method (lower panels) in small-scale model case. The location errors were projected onto the horizontal plane (left panels) and corresponding source numbers vs. location error (right panels)

inappropriateness of flat Earth ray tracing leads to inaccuracies in velocity anomalies that are greater than 1.0%. These errors are up to 0.9% for the smaller model which involves source–receiver distances slightly in excess of 200 km. The inaccuracy in positioning source locations is up to 2.0 km for the larger model and up to 1.5 km for the smaller model. The recovered Moho depth is in error by up to 1.0 and 0.5 km for the two cases, respectively. Incorrect images also appear in the recovered velocity tomograms. The numerically simulated inversion results for both 3-D models show that one should use spherical coordinates and spherical Earth ray tracing if there are an appreciable number (say 20%) of rays having epicentral distances greater than 150 km.

Regarding to how to select the cutoff in error, one should consider in real application. In our case, if we assume that averaged P-wave velocity here is 6.0 km/s, and then for velocity model, the 0.5% inaccurate image will result in ±0.3 km/s P-wave perturbation; for determining the earthquake hypocenters, the cutoff is 1 km in distance, which results in traveltime error of ±0.17 s and for Moho depth perturbation, the cutoff is ±0.3 km in vertical distance, which results

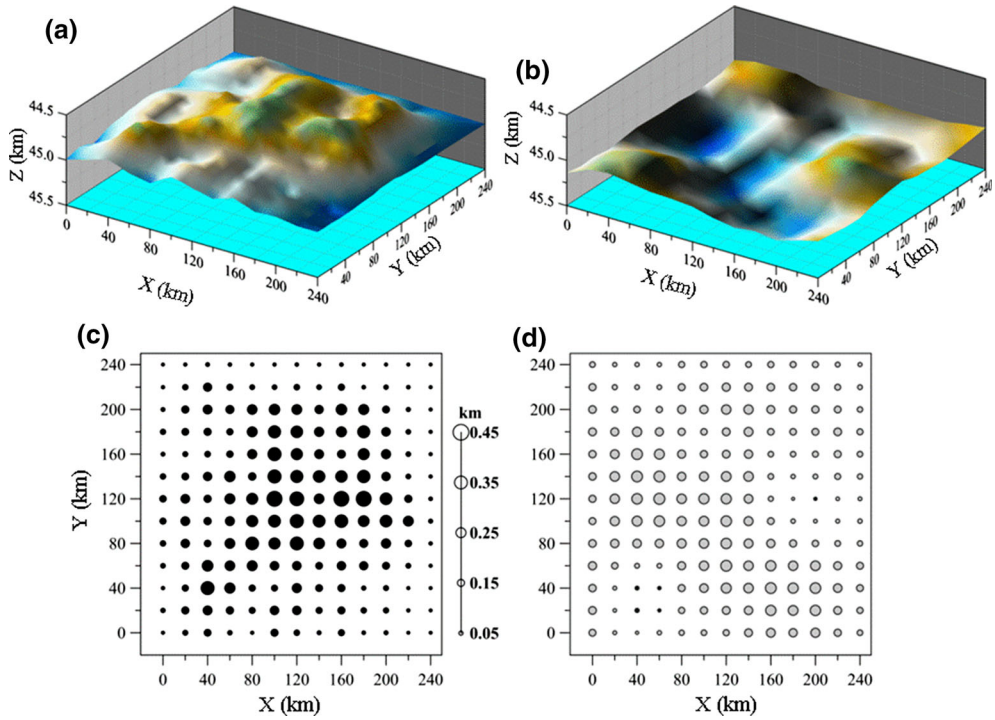

Figure 13
Updated Moho interface depth for the R_{Invert} (**a**) and $V + R$ (**b**) methods and the differences between updated and true depths (**c**, **d**) in small-scale model case. In **c** and **d**, the gray or black circles indicate positive and negative vertical distances between the updated and true reflector, and the radius of the circle denotes corresponding magnitude

Table 1

Maximum errors in the inverted quantities for three kinds of model parameters in each inversion strategy

	V_{Invert}	S_{Invert}	R	$V + R$	$V + S$
Velocity (%)	0.88 (1.06)	–	–	0.84 (0.92)	0.75 (0.91)
Location (km)	–	1.32 (2.40)	–	–	0.21 (0.33)
Interface (km)	–	–	0.43 (1.17)	0.30 (0.50)	–

In the table the number in brackets indicated the corresponding results for the large model in the Sect. 4.1

in at least traveltime error ±0.1 s if the ray is normal incident.

In the above discussion, the picking errors (normally ±0.1 s for P and ±0.2 s for PmP) were not accounted for and only the flat (1-D) crustal model was considered. It is expected that the distortions and picking errors will be even larger when dealing with real data (Zhao and Lei 2004).

References

Bai, C. Y., Huang, G. J., Li, X. W., & Greenhalgh, S. (2015). 3-D Simultaneous traveltime inversion for velocity structure, hypocenter locations, and reflector geometry using multiple classes of arrivals. *Pure and Applied Geophysics, 172,* 2601–2620.

Bai, C. Y., Huang, G. J., & Zhao, R. (2010). 2-D/3-D irregular shortest-path ray tracing for multiple arrivals and its applications. *Geophysical Journal International, 183,* 1596–1612.

Bozdağ, E., & Trampert, J. (2010). On crustal corrections in surface wave tomography. *Geophysical Journal of the Royal Astronomy Society, 172,* 1066–1082.

Chapman, C. H. (1973). The Earth flattening transformation in body wave theory. *Geophysical Journal of the Royal Astronomy Society, 35,* 55–70.

Gorman, A. R. (2002). Ray-theoretical seismic traveltime inversion: modifications for a two-dimensional radially parametrized Earth. *Geophysical Journal International, 151,* 511–516.

Gorman, A. R., Clowes, R. M., Ellis, R. M., Henstock, T. J., Spence, G. D., Keller, G. R., et al. (2002). Deep Probe: imaging the roots of western North America. *Canadian Journal of Earth Sciences, 39,* 375–398.

Gruber, T (1998) *Crosshole seismic tomography incorporating later arrivals*. Ph.D. thesis, The University of Adelaide.

Huang, G. J., Bai, C. Y., & Greenhalgh, S. (2013). Fast and accurate global multiphase arrival tracking: the irregular shortest-path method in a 3-D spherical earth model. *Geophysical Journal International, 194,* 1878–1892.

Huang, G. J., Bai, C. Y., Zhu, D. L., & Greenhalgh, S. (2012). 2D/3D seismic simultaneous inversion for velocity model and interface geometry using multiple classes of arrivals. *Bulletin of the Seismological Society of America, 102,* 790–801.

Kennett, B. L. N., & Engdahl, E. R. (1991). Traveltimes for global earthquake location and phase identification. *Geophysical Journal International, 122,* 429–465.

Kennett, B. L. N., Engdahl, E., & Buland, R. (1995). Constraints on seismic velocities in the Earth from traveltimes. *Geophysical Journal International, 122,* 108–124.

Kennett, B. L. N., Sambridge, M. S., & Williamson, P. R. (1988). Subspace methods for large inverse problems with multiple parameter classes. *Geophysical Journal International, 94,* 237–247.

Li, X.W., Bai, C. Y., Wang D. & Greenhalgh S (2017) Ray tracing in a 3-D ellipsoidal Earth model for multi-phase global arrivals. Bulletin of the Seismological Society of America **(under revision)**.

Müller, G. (1971). Approximate treatment of elastic body waves in media with spherical symmetry. *Geophysical Journal Royal Astronomy Society, 23,* 435–449.

Rawlinson, N., & Sambridge, M. (2004). Multiple reflection and transmission phases in complex layered media using a multistage fast marching method. *Geophysics, 69*, 1338–1350.

Snoke, J. A., & Lahr, J. C. (2001). Locating earthquakes: at what distance can the Earth no longer be treated as flat. *Seismological Research Letters, 72,* 538–541.

Squires, L. J., Blakeslee, S., & Stoffa, P. L. (1992). The effect of statics on tomographic velocity reconstructions. *Geophysics, 57,* 353–362.

Zhao, D. P., & Lei, J. S. (2004). Seismic ray path variations in a 3D global velocity model. *Physics of the Earth and Planetary Interiors, 141,* 153–166.

Zhou, B., Greenhalgh, S. A., & Sinadinovski, C. (1992). Iterative algorithm for the damped minimum norm, least-squares and constrained problem in seismic tomography. *Exploration Geophysics, 23,* 497–505.

(Received February 27, 2017, revised July 8, 2017, accepted September 10, 2017, Published online September 26, 2017)